Lotus Leaf Structured Fluoropolymer Foils for Superhydrophobicity and Enhanced Light Management in Photovoltaic Devices

D. Yoo, S. Garud, C. T. Trinh, D. Amkreutz, C. Becker

Abstract— **Reflection losses and soiling of photovoltaic devices are well known challenges that suppress their full operational potential. Multifunctional self-cleaning light management foils offer a concurrent solution to both subjects. Here we demonstrate a simple processing method to fabricate a lotus leaf textured fluoropolymer foil by nanoimprint lithography and hot embossing. We employ nanoimprinted molds for hot embossing, bypassing the conventional electroforming process to enable facile prototyping. Light management qualities as well as superhydrophobic properties are investigated by comparing non-textured foils with lotus leaf structured and random micro-pyramid foils. One dimensional optical simulation verified the anti-reflective properties of the lotus texture. Implementing the lotus leaf textured foil to the sun facing air-glass interface of liquid-phase-crystallized silicon thin-film solar cells was found to induce a broadband antireflective effect and increase the short-circuit current density J_{sc} up to 3.4% (relative). At the same time, the water contact angle of the planar glass superstrate was improved from 47° to superhydrophobic 157° by the attached lotus foil.**

Index Terms—**Fluoropolymer foil, hot embossing, light management, lotus effect, nanoimprint lithography, silicon, thin-film solar cell.**

I. Introduction

THE primary light collection potential of a photovoltaic (PV) device is essentially determined by the property of its sun- and weather-facing surface. Appropriate design of the surface texture is necessary to fulfill multiple functions simultaneously. In the ideal case, the front surface consists of a weather-stable and industrially relevant material, exhibits self-cleaning abilities, and allows minimizing optical losses.

Dust accumulations on photovoltaics modules can cause considerable optical and electrical losses, with the consequence of reduced power generation, if not treated in time[1]–[3]. This issue has been addressed by various approaches ranging from active measures such as manual cleaning, robot cleaners to passive self-cleaning solutions like anti-soiling spray coatings or implementation of superhydrophobic textures [4]–[7]. Latter are characterized by large water contact angles (CA) (>150°) and small roll-off angles (RA) (<10°), forming a highly water-repellent surface that enables dust particles to be flushed down with the help of water [8], [9]. Especially the RA is an essential factor for self-cleaning function, as it determines the critical tilting angle, upon which the water droplet begins to slide down a surface. Therefore, the RA of a self-cleaning PV surface must be designed to be smaller than the tilt angle of the module.

The described surface properties can be found in many organic surfaces of plants which naturally develop hierarchical structures, a thoroughly studied prerequisite for superhydrophobic surfaces [10]. On superhydrophobic surfaces, water droplets are in the Cassie-Baxter regime, in which the structural cavities underneath the droplet are filled with air, minimizing the contact area between liquid and surface [11]. This enables the droplets to easily roll-off the surface and form a fundamental component for self-cleaning.

In addition, these organic textures were reported to not only exhibit excellent self-cleaning, but also to reduce reflection losses and hence significantly improve the optical performances when employed to solar cells [12], [13]. For this reason, various types of bio-inspired [14]–[18] and bio-replicated [19]–[21] textures have been investigated in the context of photovoltaics. Some studies investigated bio-replicated plant leaf structures on solar cells solely for optical reasons [22], [23]. Among bio-inspired structure templates lotus leaves (*Nelumbo nucifera*) are especially attractive due to their hierarchical double-texture, which excels in both optical properties as well as self-cleaning function, providing a multifunctional solution for PV [12], [19], [24]–[29]. Inspired by the lotus texture, various microfabrication processes were developed to create an artificial double-texture and exploit its light-scattering ability for anti-reflection as well as anti-wetting properties [28], [30], [31]. Furthermore, its abundance and the leaves reaching diameters of up to 80 cm, create an optimal platform for large scale reproduction in photovoltaics [32].

To become a relevant solution for PV, multifunctional textures must be present in a material, which can withstand the demanding environmental and operational conditions of the real world. Efficient light management foils on various PV technologies have been proposed but the industrial applicability

This work was supported by the European Regional Development fund and the state government of North Rhine-Westphalia in the framework of the Up-LLPC Project (grant nos. EFRE-0800580 and EU-1-2-037C)

D. Yoo, S. Garud, C. T. Trinh, D. Amkreutz, C. Becker are with Helmholtz-Zentrum Berlin für Materialien und Energie GmbH, D-12489 Berlin, Germany (e-mail: danbi.yoo@helmholtz-berlin.de; siddhartha.garud@helmholtz-berlin.de; cham.trinh@helmholtz-berlin.de; daniel.amkreutz@helmholtz-berlin.de; christiane.becker@helmholtz-berlin.de).

of the investigated materials is often times neglected [33]–[36].

In this context, thermoplastic fluoropolymers foils have become increasingly the material of choice, as they offer application flexibility, excellent chemical and mechanical durability, as well as optical properties, highly suitable for PV application [14], [16], [20], [37]–[40]. Even simple fluoropolymer nano-coatings on glass were shown to be anti-reflective due to their low refractive indices, softening the optical transition in the air/glass interface [41], [42]. Additionally, non-textured fluoropolymers were reported that exhibit hydrophobic contact angles (>90°) arising from their low surface energy [16], [41], [43]–[45]. Implementing textures was described not only to improve anti-wetting properties but also to improve broadband anti-reflection due to light scattering [14], [37]. Furthermore, being already established materials in the construction industry, the availability and reliability of fluoropolymers are also assured [46]

To date, the conventional method of micro replication in thermoplastic fluoropolymers is based on hot embossing, a compression molding process in which a polymer film is heated to its melting range and compressed into a microstructured mold. Starting from the basic plate-to-plate setup to high throughput modifications such as roll-to-plate or roll-to-roll embossing, a variety of technologies have emerged [47].

However, conventional hot embossing machines involve the use of large embossing forces combined with electroformed metal mold inserts, which can withstand the exposed forces. Electroforming of microstructures is a delicate process that requires precisely controllable electroplating equipment for reliable results and long deposition times, especially for the macroscopic thickness (several millimeters) needed [48]–[53]. Alternative molds, so called “intermediate mold inserts” in polymer materials have been reported to enable rapid prototyping in research applications [54]–[56].

A faster and accessible mold replication process, avoiding long-lasting electroforming processes and the option to work with reduced forces would greatly facilitate research and development of bioinspired foils for photovoltaic modules.

In this work, we demonstrate a facile fabrication process, replicating the texture of lotus leaves and random pyramidal textures to fluoropolymer foils with areas up to 36 cm^2 by means of nanoimprint lithography (NIL) and hot embossing. By employing reusable nanoimprinted glasses as alternative mold inserts, we provide a time-efficient and simple processing method for prototyping structured fluoropolymer foils for PV application. Via contact angle measurements we demonstrate superhydrophobic behavior of the lotus leave structured fluoropolymer foils. We further investigate light management qualities of lotus leaf and random pyramidal microstructures in optical simulations as well as in experiment. We modularly attach the microstructured foils to liquid-phase crystallized silicon (LPC-Si) solar cells and analyze their reflectance, external quantum efficiency and current-voltage characteristics. The fundamental experimental characteristics were studied in a previous conference proceeding [57]. The present work complements the foregoing study with detailed information on the processing scheme and analysis of the replication process.

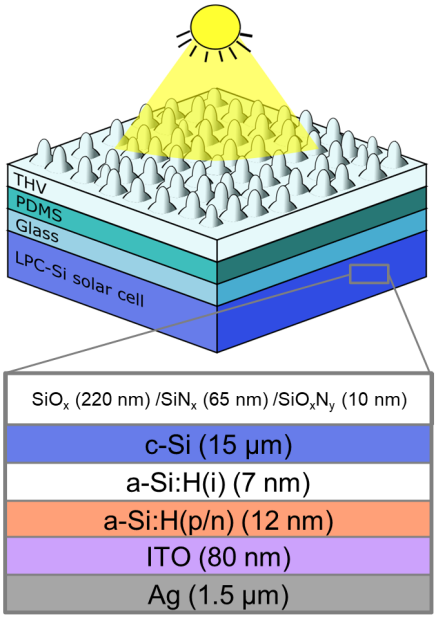

Fig. 1 Schematic illustration of the illuminated glass superstrate configuration of the solar cell with THV lotus foil attached with PDMS. The detailed layer stack of the solar cell is given in the grey inset. Note that the colored layers are highlighted due to their relevance in the optical simulation (cf. **Fig. 7**)

Moreover, optical simulations are performed to quantify the optical performance of the lotus structure. The experimental data is expanded with supplementary characterization of additional solar cells to demonstrate the modular nature and flexibility of the light management foils.

II. METHODS

A. Solar Cell Fabrication

High performance LPC-Si solar cells require buffer layers between silicon and the glass substrate, appropriate crystallization conditions and an optimized contacting scheme. In this work, two different solar cells with varying doping levels of the silicon absorber are fabricated, which are referred to device A and B. First, a layer stack of 220 nm SiO_x /65 nm SiN_x/10 nm SiO_xN_y is deposited on Eagle XG glass substrates (Corning) via plasma-enhanced chemical vapor deposition (PECVD). This multifaceted layer stack has been discussed in [58]. Secondly, electron-beam evaporation is used to deposit intrinsic silicon of the desired thickness (15 - 17 µm in this work) at a high rate of deposition (600 nm/min). Next, the desired doping is introduced by the deposition of a dopant source via PECVD, which is 80 nm of phosphorous doped a-Si:H(n+) layer in this case. Doping of the bulk silicon occurs during the liquid-phase crystallization and is measured to be 7.7 $\pm$ 2.7 $\times$ 10^{16} cm^{-3} and 1.0 $\pm$ 0.6 $\times$ 10^{16} cm^{-3} for device A and B, respectively. Previous studies have demonstrated the significance of doping levels on vital device properties [59]. Finally, 100 nm of SiO_x is deposited as a capping layer, which prevents agglomeration and dewetting during the crystallization process. The silicon bulk is crystallized with a line-shaped,

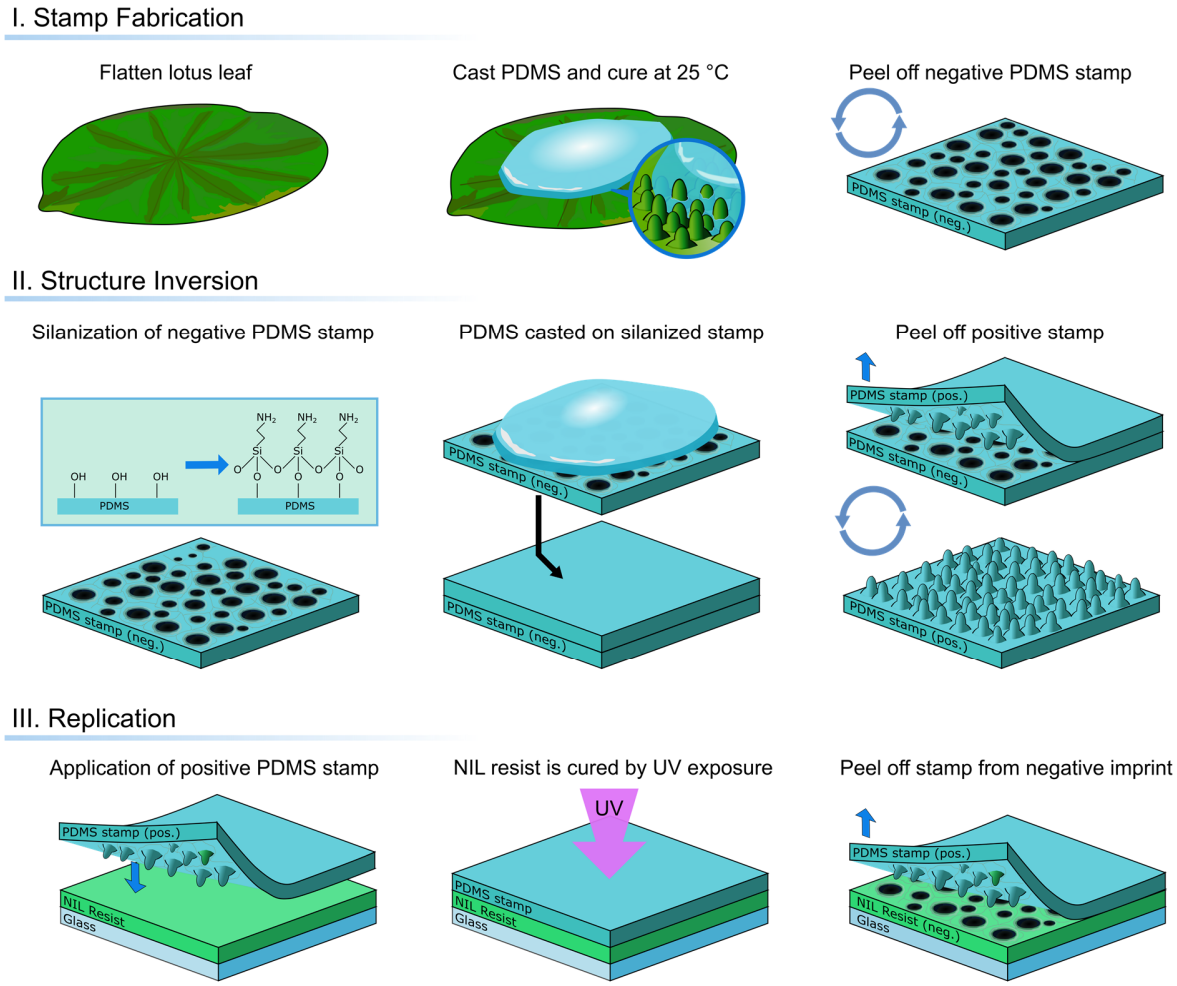

Fig. 2 Schematic illustration of lotus leaf texture replication with via soft lithography and subsequent pattern inversion. **I.** Fresh lotus leaf is flattened on a glass substrate and replicated with PDMS. **II.** PDMS stamp is immersed in Sigmacote to form antiadhesive layer on the surface. Subsequent PDMS casting on the silanized PDMS stamp and thermal curing process results in a positive stamp. **III.** Nanoimprinted mold fabrication sequence via UV-NIL. An even layer of Ormocomp is applied to the glass substrate. The inverted positive stamp is then placed on the resist and cured under UV exposure. After thermal curing, the negative lotus imprint is a ready-to-use mold insert.

continuous-wave diode laser with a wavelength of 808 nm and power density of 1.48 kW/cm^2. Details of all chemical cleaning, texturing and etching steps can be found in [60]. The contacting layers are based on a silicon heterojunction interdigitated back contact architecture (SHJ-IBC). It requires two PECVD steps and three photolithography steps. Cells with a designated illumination area of 1 cm × 0.6 cm were made on 5 cm × 5 cm substrates. Some areas of the electron contact were laser-fired to reduce contact resistance [61]. For more details on contact fabrication and laser firing, the reader is referred to [60], [62].

B. Nano-imprint Lithography and Structure Inversion

Multifunctional lotus light management foils are fabricated by first replicating the biotexture via nano-imprint lithography (NIL) and subsequently transferring the structure via hot embossing to the target material. **Fig. 2** displays the initial stamp fabrication process, in which a freshly cut leaf of *Nelumbo nucifera* (Botanischer Garten Berlin) is flattened on a glass substrate using a double-adhesive tape.

A layer of liquid poly-dimethyl siloxane (PDMS) (Wacker), mixed in a matrix to crosslinker ratio of 9:1, is cast to the prepared lotus leaf and cured for 24 h at room temperature. The PDMS stamp carrying the negative lotus texture is peeled off and cut to a 6 x 6 cm^2 square. To fabricate a lotus foil carrying the positive structure via hot embossing, a negative of the master structure is required, as the structure is inverted during the process. Therefore, the cast lotus stamps are inverted via solution based silanization and subsequent soft lithography to fabricate a negative lotus imprint. The lotus stamp is first surface activated with an oxygen plasma provided by an inductively coupled reactive ion etcher (ICP-RIE) (Plasmalab 8000, Oxford Instruments). Following processing parameters were used: ICP power of 100 W, RF-power 200 W and a forward bias of 100 V, t = 1 min.

The surface activated PDMS stamp is then immersed in the siliconizing solution Sigmacote (Sigma-Aldrich) until fully saturated and air-dried in a fume hood. Sigmacote is a solution of heptane and 1,7-Dichloro-1,1,3,3,5,5,7,7 octamethyl-tetrasiloxane. In the last step, a liquid PDMS mixture (9:1 ratio)

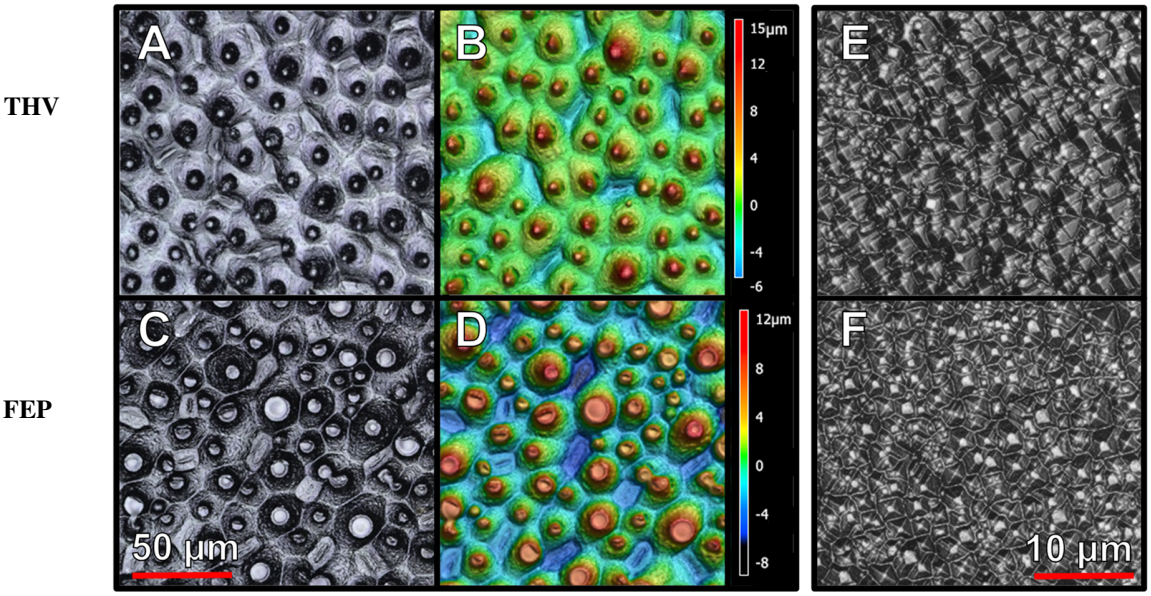

Fig. 3 Confocal laser scanning microscope images of THV lotus foils (**A**) in laser image and (**B**) overlayed with height information**.** Incomplete, "cut off" structure of FEP lotus foils (**C**) in laser mode and (**D**) overlayed with height information. Pyramid structure recorded with 150× magnification in (**E**) THV and (**F**) FEP.

is cast onto the silanized PDMS stamp and cured for 20 min at 70 °C. A covalent thin-film anti-adhesive layer is formed and the positive PDMS stamp can be separated from the silanized stamp.

In the third stage the UV curable NIL-resist Ormocomp (microresist technology) is applied to a 10 x 10 cm^2 Eagle XG (Corning) glass substrate and evenly distributed with a custom-made blade coater. The inverted PDMS stamp is then carefully applied to the resist and illuminated with UV light for 10 min. It is crucial to avoid any formation of air bubbles at this stage. After the exposure, the lotus imprint (negative texture) is thermally cured for 20 min at 130 °C. The fabricated artificial lotus leaf serves as mold insert in the final hot embossing step.

C. Hot Embossing

Fluoropolymer foils are hot embossed with the nanoimprinted lotus mold inserts. The foils are heated close to the melting point and the texture is transferred by applying a loaded force. In this work, two variations of fluoropolymers are investigated, namely fluorinated ethylene propylene (FEP) (refractive index n = 1.34) (DuPont) (d = 127 µm) and the terpolymer of tetrafluoroethylene, hexafluoropropylene and polyvinylidenefluoride (THV) (nowofol) (refractive index n = 1.36) (d = 150 µm).

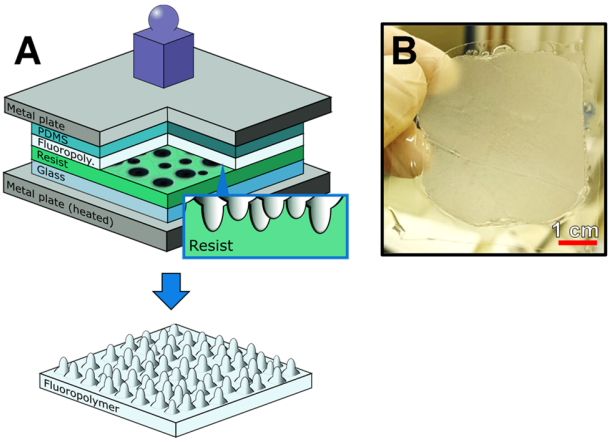

Fig. 4 A Schematic illustration of embossing stack clamped between two metal plates with 100 N load and resulting embossed fluoropolymer with positive lotus structure. **B** Photograph of 5 × 5 cm^2 lotus foil in THV.

The texture transfer is carried out with a custom-made embossing setup, which allows clamping the embossing stack between two metal plates as shown in **Fig. 4A**. The imprinted negative master is placed on the lowest level, followed by the fluoropolymer and a layer of planar PDMS on top. Latter ensures an even distribution of the loaded force and levels out the naturally occurring waviness of the lotus leaf (especially at the leaf veins). Beginning at a material specific starting temperature (Table I), the clamped embossing stack is heated on a conventional laboratory hot plate at a ramping rate of 12.5 °C/min and loaded with a force of 100 N and held for 5 min upon reaching the target embossing temperature. Note that the small load preserves the simplicity and feasibility of the process with imprinted mold inserts using standard laboratory equipment. The setup is then cooled down for a minimum of 30 min before the embossed foils are peeled off the master. In the final step, the embossed foils are reinserted in the embossing setup clamped between two planar PDMS layers to flatten the foil for 5 min at elevated temperatures (Table I) [45].

Pretests suggested that the adjusted temperature of the hot plate deviated by approx. 40 °C from the experimentally determined melting temperatures. This effect can be attributed to heat dissipation in air and the metal plates. The specified embossing temperatures are therefore according to the hotplate display.

TABLE I
VARIOUS PROCESSING TEMPERATURES FOR HOT EMBOSSING FEP AND THV

	Melting Temperature	Starting Temperature	Embossing Temperature	Flattening Temperature
FEP	270 °C	100 °C	330 °C	125 °C
THV	125 °C	75 °C	175 °C	90 °C

D. *Characterization*

The surface topography of the NIL-replicated and embossed lotus textures was investigated with a Keyence VKX400 confocal laser scanning microscope. The morphological properties of the microscopic images were determined with the software MultiFileAnalyzer (Keyence). Using the drop shape analyzer DSA25B (Krüss) water contact angles were determined with the Young-Laplace equation. To determine the corresponding water roll-off angles, a digital protractor Acromaster 40 (Laserliner) was mounted to the sample stage. RA was then analyzed depositing 13 µl water droplets and tilting the protractor at a tilting rate of ca. 3° per second until the droplet started to creep down the surface. For solar cell characterization, the embossed fluoropolymers were adhered with a thin layer of PDMS on the sun facing glass superstrate of the LPC-Si solar cells, which is schematically illustrated in **Fig. 1**. Current-voltage characteristics were measured with a WXS-156S-L2 class AAA solar simulator of Wacom Electronic Company under one sun AM1.5g illumination. Transmission and reflectance properties were analyzed with a PerkinElmer Lambda 1050 photo-spectrometer. External quantum efficiency (EQE) was measured with a custom-made setup with an illumination area of 10 × 10 cm^2.

E. *Simulation*

The simulation software GenPro4 was used to perform optical loss simulations. Textured surfaces are considered by implementing ray and wave-optics to generate a scatter matrix from the height profile of the lotus structure. The photon absorption profile in the absorber material is treated as a 1-D cross-section. Refractive indices were adapted from the native database of GenPro4 and from ellipsometry studies [63][64].

III. RESULTS & DISCUSSION

A. *Fabrication Process*

In the first step we evaluate the results of the embossing process by microscopic analysis of the replicated textures. To assess the relative performance of the fabricated lotus foils, both materials were additionally embossed with micropyramid imprints. The micropyramids were imprinted from potassium hydroxide etched silicon wafers.

Fig. 3A-D displays the microscopic topography for both lotus embossed materials. The embossed lotus texture in THV (**Fig. 3A, B**) is characterized by randomly distributed bio-cones, each greatly varying in size and shape. The structural properties

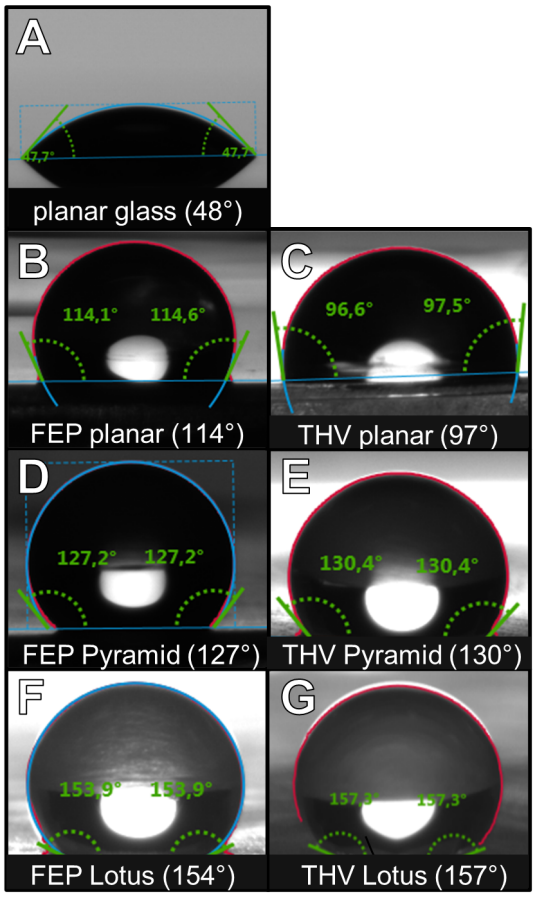

Fig. 5 Water contact angles approximated by Young-Laplace equation for (**A**) planar glass, (**B**) FEP planar, (**C**) THV planar, (**D**) FEP Pyramid, (**E**) THV Pyramid, (**F**) FEP Lotus (incomplete, "cut off" structure), (**G**) THV Lotus.

are conformal to previously taken images of lotus leaves, underlining a successful replication of the lotus texture. In contrast, the FEP lotus foils in **Fig. 3C, D** show a significant structural deficiency compared to the master structure. Although the basic features of the lotus structure are recognizable, it is noticeable that the sharp tips of the bio-cones are predominantly missing. Feature size analysis (peak to valley) on the investigated surface area show the average height of bio-cones in the lotus master structure to be 11.1 µm. A corresponding analysis reveals that THV lotus foils reach 91% (8.3 µm) of the average height, while the average size in FEP is found to reach only 75% (7.3 µm). The replicated micropyramids depicted in **Fig. 3E, F** show similar trends to the prior measurements. A large part of the pyramids in FEP (**Fig. 3F**) are replicated with incomplete formation of the tips. Equivalent feature size analysis shows the pyramid master structure average height to be 0.9 µm. This value is reached by 95% (0.85 µm) in THV foils, while the FEP pyramids reach 88% (0.79 µm) of the original height. A high comparability of the morphology was ensured by introducing scratch marks to the master structures prior to hot embossing and enabling the analysis of identical sample areas. Therefore, the described statistical evaluation provides a good orientation for the

reproduction quality. Based on the microscopic analysis of the fabricated foils we conclude that our processing setup is well suited to transfer the lotus and pyramid structure to THV with surface areas of up to 6 x 6 cm^2, but not sufficient to fully replicate same structures in FEP. Due to the high melting point of FEP and considering the aspect ratio of the lotus structure, an embossing force several magnitudes higher is suggested [65].

B. Contact Angle & Roll-off Angle Measurements

To investigate lotus foils as potent multifunctional module cover sheets we assess the wetting property by static contact angle and roll-off angle measurements. The contact angle of both materials FEP and THV with varying surface structures are depicted in **Fig. 5** and selected roll-off angle measurements in **Fig. 6**. The glass surface of the planar reference cell shows hydrophilic property in which the CA is 48°. Non-textured THV foils exhibit hydrophobic CA of 97° and large RA of 84°. In comparison, non-textured FEP foil is intrinsically more hydrophobic with a higher CA of 115° and RA of 43°. This strongly emphasizes the importance of the intrinsic surface energy of the chosen material, but the RA measurements also illustrate that hydrophobic contact angles are not necessarily associated with small roll-off angles. With the introduction of pyramid textures, the CA improves to 130°, but increases RA >90°. Here, the droplet is pinned to the surface and remains stable in this state beyond 90°. The same structure increases the CA in FEP to 127° and reduces the RA to 31°. This is an improvement of the RA by 10° compared to non-textured FEP. Finally, by implementing the lotus texture in THV results in a superhydrophobic CA of 157° but also leads to pinning of the water droplet and hence a RA >90° (Fig. 6D). FEP textured with cut off lotus texture, also exhibits a superhydrophobic contact angle of 154° and RA >90°.

The phenomenon of pinned droplets can be explained by a wetting transition from the Cassie-Baxter state to the Wenzel state, in which water penetrates the cavities of the underlying texture. Structuring THV, which intrinsically exhibits large RA, lowers the wetting transition barrier, favoring the Wenzel state and thereby worsening the RA [66].

However, to test the effect of a fully replicated lotus structure in FEP, the embossing temperature was increased from 330 °C to 350 °C, while the force was kept constant. As shown in **Fig. 6F** the adjusted processing temperature results in a low RA of 8° along with a high CA of 158°. These values are comparable to fresh lotus leaves in nature [67], [68]. These results are also in line with the observations from [45], which reports the correlation of roll-off angle and embossing temperature, as this contributes significantly to the quality of the structure replication.

To assess the actual self-cleaning function, extensive tests are required to simulate the soiling and cleaning behavior with realistic environmental conditions. These tests will be the subject of future work.

C. Optical Simulations

The lotus surface profile measured with confocal laser scanning microscope was used to approximate the textured interface and generate an optical scatter matrix. This allowed us to calculate absorption, reflection, and transmission in the LPC-Si solar cell layer stack (**Fig. 1**). To quantify the optical solar cell performance, we calculated implied photocurrents J_{ph} by integrating the corresponding reflection, transmission, and absorption in the absorber and supporting layers over the AM1.5 solar spectrum.

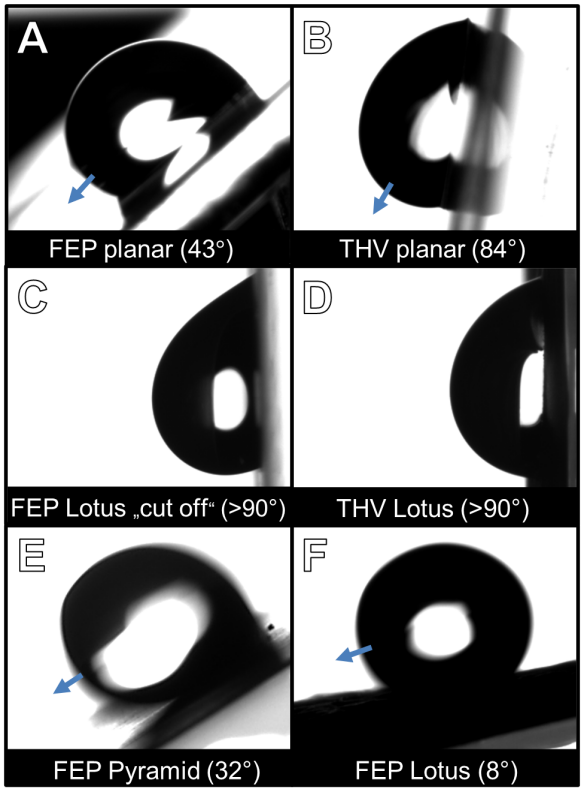

Fig. 6 Water roll-of angle measurements with 13 µl droplet for (**A**) FEP planar, (**B**) THV planar, (**C**) FEP Lotus (incomplete, "cut off" structure), (**D**) THV Lotus, (**E**) FEP Pyramid, (**F**) FEP Lotus.

$$J_{ph-i} = e \int_{300\,nm}^{1200\,nm} \Phi_{\mathrm{AM1.5}}(\lambda)\, A_i(\lambda)\, d\lambda \qquad (1)$$

where e is the elementary charge, $\Phi_{\mathrm{AM1.5}}(\lambda)$ the spectral photon flux under AM1.5 illumination, A_i the absorption in the i^{th} layer in the device. For detailed information on the modelling theory, please refer to [63], [69]–[71].

The simulation of the planar reference and lotus foil attached device are illustrated in **Fig. 7**. Implementing the lotus foil, a significant improvement is observed in the blue area, in which the absorptance of the LPC-Si absorber layer is enhanced by 2.2 mA/cm^2 compared to the reference device. The increased absorption can be attributed to three factors improving the light in-coupling at the front surface. The first fundamental antireflective effect arises from using a stack of low index materials. Due to the lower refractive index of THV (n = 1.36) relative to the underlying layer of PDMS (n = 1.43) and glass (n = 1.51), a graded index effect is introduced. The second

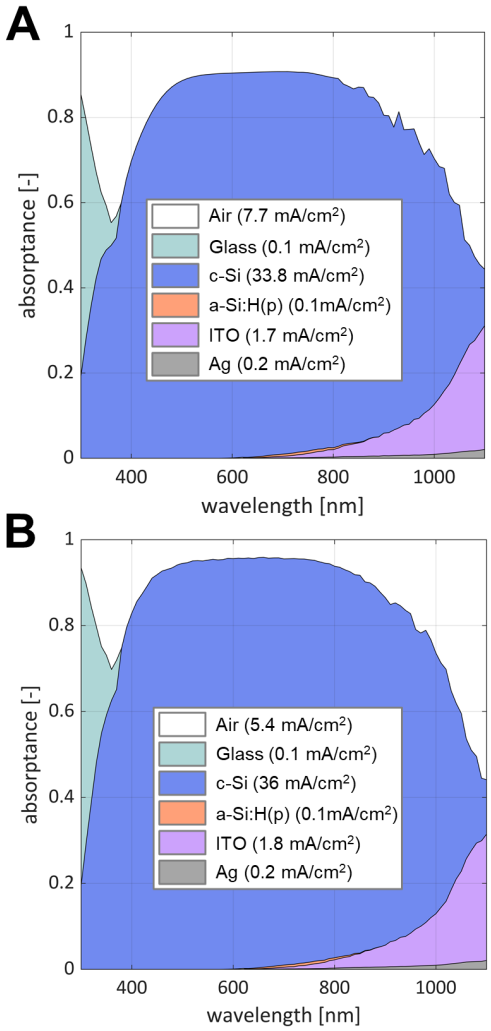

Fig. 7 1-D simulation optical loss analysis for **(A)** planar reference and **(B)** lotus foil attached LPC-Si solar cell. The insets show photocurrent generation and loss profiles derived from the absorption spectra.

contribution comes from the presence of scattering structures, which increase the probability of reflected photons to be redirected to the surface, rather than being backscattered to the air. The third factor is light trapping, in which photons are scattered at the lotus structure giving rise to light path enhancement in the solar cell absorber layer.

D. Solar Cell Characteristics

After calculating the potential optical loss reduction, we experimentally assessed the light management effect of the structured fluoropolymer foils laminated on LPC-Si solar cells. Due to the better structural fidelity in THV with the fabrication method presented here and highly comparable optical properties of THV and FEP, LPC-Si solar cells were assembled and characterized with THV. For comparability and validation of the foils, we employ two different LPC-Si solar cells referred to devices A and B. For detailed information on both devices the reader is referred to section II.A. For quantification of the

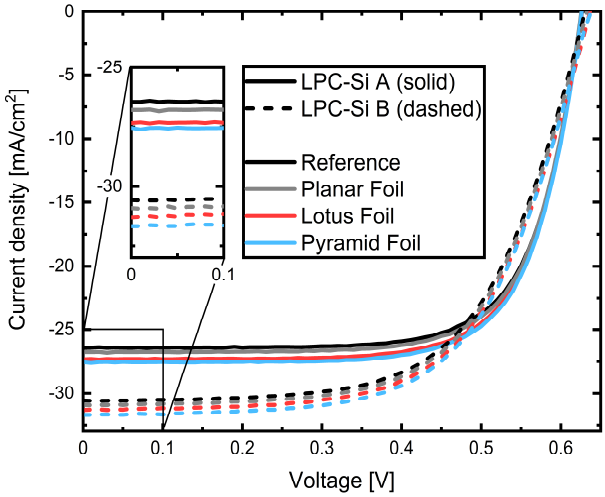

Fig. 8 *J-V* characteristics of LPC-Si solar cells A (solid lines) and B (dashed lines) in planar configuration without foil (black), attached with lotus (red), pyramid (blue) and planar THV foil (gray). The inset shows a detailed view of J_{SC} for better clarification.

antireflective effect solely arising from the low index material, untextured THV foils were incorporated. To assess the relative performance of lotus foils in comparison to already established light management structures, THV was also embossed with micropyramids, imprinted from potassium hydroxide etched silicon wafers. Due to the modular nature of the foils, the measurements were performed each time on the identical cell by reversibly attaching 1.5 × 1.5 cm² foils, sufficiently large to cover the active area, with PDMS to the sun facing glass superstrate of the solar cell. This ensured the best possible comparability. First, the effect of each foil on the electrical performance is analyzed by recording current density-voltage (*J-V*) characteristics. **Fig. 8** shows *J-V* characteristics for each foil variation implemented to both devices A (solid lines) and B (dashed lines). Improvements of the current density J_{SC} and the corresponding increase in power conversion efficiency (PCE) are observed for all set of foils compared to the planar reference without foil in both measured devices. For device A, implementing the planar THV foil already increases J_{SC} from 26.4 mA/cm² to 26.8 mA/cm², corresponding to a gain of 1.5%. By texturing the foil J_{SC} is further increased to 27.3 mA/cm² (3.4%) and 27.5 mA/cm² (4.2%) for the lotus and pyramid structure, respectively. Detailed device properties are summarized in Table II. For the second device B, which has an intrinsically higher J_{SC} of 30.6 mA/cm², the planar THV foil improves the current density from 30.6 mA/cm² to 30.9 mA/cm² (1%), whereas employing the lotus and pyramid foils enhance J_{SC} to 31.3 mA/cm² (2.3%) and 31.7 mA/cm² (3.6%), respectively. In both devices a significant gain in device performance can be attributed to the implemented surface

textures. The structure dependent antireflective effects, as discussed in section III.C, are quantified by the relative J_{SC} gain of both structured foils to the planar THV devices.

The relative gain achieved in similar works employing textured fluoropolymer foils, is in the same order of magnitude. Despite of using different PV architectures such as CIGS and multicrystalline silicon modules, the relative gain of short-circuit current and current density were ranging from 3.1 – 4.6% [14], [37].

To further resolve enhanced light in-coupling and improved device characteristics, 1-Reflectance (1-*R*) and EQE measurements are presented in **Fig. 9**. All employed foils promote broadband antireflective effects as concluded from the 1-*R* measurement. The highest reduction of reflection is achieved by the pyramidal textured foil, closely followed by the lotus textured foil. As expected, even the planar THV foil records a small reduction of reflection. Furthermore, the broadband antireflective effect translates to improved EQE in all devices compared to the planar reference (without foil). The optical measurements coincide with the observations from the current-voltage characteristics (**Fig. 8**) in which the pyramid structure is performing marginally better than the lotus foil. A substantial difference between both structured foils and the non-textured foil underlines the additional optical enhancement solely arising from the structures.

The experimentally quantified device improvements also agree with the 1-D optical simulations shown in **Fig. 7**. Note that absolute values from experiment and simulations may differ as latter is a purely optical model to calculate the maximum achievable short circuit current, neglecting electrical device properties such as charge carrier collection and thereby assuming an internal quantum efficiency of unity.

A comprehensive study on the angle dependent optical performance of the lotus foil and the resulting device performance is in progress and will be the subject of our future work.

TABLE II
SOLAR CELL PARAMETERS OF LPC-SI SOLAR CELLS DEVICE A AND B WITH MODULAR AR FOILS ATTACHED TO THE AIR-GLASS INTERFACE.

Device		J_{SC} [mA/cm^2]	ΔJ_{SC} [%]	V_{OC} [V]	Fill Factor [%]	PCE [%]
A	Reference	26.4	-	0.63	71.6	11.9
	Planar Foil	26.8	1.5	0.63	71.7	12
	Lotus Foil	27.3	3.4	0.63	71.8	12.3
	Pyramid Foil	27.5	4.2	0.63	71.6	12.4
B	Reference	30.6	-	0.63	62	11.9
	Planar Foil	30.9	1	0.63	61.7	12.1
	Lotus Foil	31.3	2.3	0.63	61.5	12.3
	Pyramid	31.7	3.6	0.63	61.2	12.4

IV. CONCLUSION

In this work we have demonstrated the fabrication and integration process of fluoropolymer foils with bio-replicated lotus leaf structure to LPC-Si solar cells. We showed that the characteristic microstructure of lotus leaves exhibits

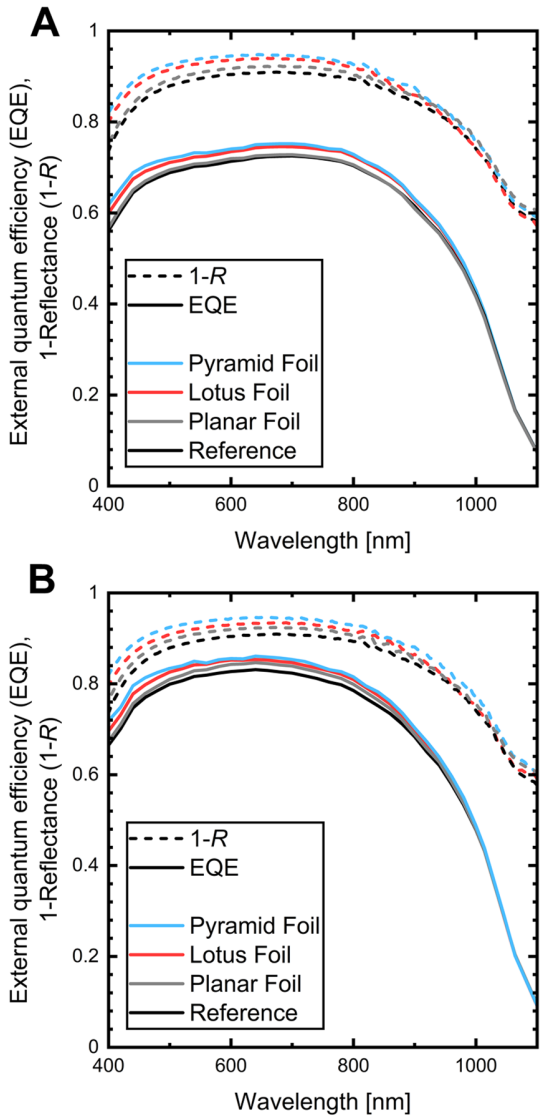

Fig. 9 External quantum efficiency and 1-Reflectance of (**A**) device A and (**B**) device B, both attached with lotus (red), pyramid (blue) and planar (grey) foil - the reference device is represented by the black line.

multifunctional properties by optically enhancing device performances and forming superhydrophobic surfaces. We specifically configured the processing setup to enable hot embossing with nanoimprinted mold inserts for fast prototyping bio-replicated light management foils. To match such conditions, the applied force was fixed to 100 N, sufficient to replicate foils of up to 6 × 6 cm^2. Structural analysis via CLSM revealed that the lotus structure was replicated with much higher fidelity in THV than in FEP, where the structural features were predominantly cut off.

Attaching the THV lotus foil led to a broadband reduction of reflection and increased the short-circuit current density of solar cell devices up to 3.4% (relative). This is slightly below the performance of pyramid structured foils used as reference, which increased the short-circuit current by 4.2%. Optical loss analysis using the 1-D simulation software GenPro4 confirmed the antireflective effect of lotus structured fluoropolymers,

predicting a theoretically higher potential gain by 6.2%.

Contact angle and roll-off angle measurements have revealed the importance of the interplay between material and structure: The lotus textured foils reached superhydrophobic contact angles of 157° in THV as well as 154° in FEP, despite the structural deficiency of the latter. Nevertheless, we could not initially reproduce the small roll-off angles of the lotus leaf in either material and observed pinning of the water droplets.

Although the lotus texture was replicated with high structural resolution in THV, superhydrophobic roll-off angles could not be achieved. However, by increasing the embossing temperature, we succeeded in replicating the complete lotus texture also in FEP, which resulted in the desired superhydrophobic properties i.e., large contact angle (>155°) and small roll-off angle (8°). The increase of the process temperature was crucial, as it governs the structure resolution, especially at moderate embossing forces [48].

From this observation, we conclude that perfect patterning does not necessarily correlate with small RA, but also strongly depends on the intrinsic material properties.

Hence, lotus foils offer optical enhancements comparable to state-of-the-art light management textures, while exhibiting large self-cleaning potential if an appropriate material is chosen. Moreover, our method proved to be a facile processing routine of light management foils and offers great flexibility due to the simple setup. The investigated process can be easily adapted to a various range of bio-structures and scaled up to intermediate module sizes (30×30 cm^2), providing a platform for the technological transition to industrial production. Finally, based on our present findings we intend to conduct outdoor tests under real world conditions to quantify the effective multifunctional performance.

ACKNOWLEDGMENT

The authors thank Thomas Dürbye from the Dahlemer Saatgutbank (Botanischer Garten Berlin) for providing the lotus leaves. We thank Dr. Klaus Jäger from Helmholtz-Zentrum Berlin for support with the optical simulation software GenPro4. We also thank Martin Muske for his assistance in the fabrication process of the solar cells.

REFERENCES

[1] T. Weber, "Impact & Consequences of Soiling and Cleaning of PV Modules PI Photovoltaik-Institut Berlin AG," 2015.

[2] K. -a. W. E. Klimm, T. Lorenz, "Can Anti-Soiling Coating on Solar Glass Influence the Degree of Performance Loss over Time of PV Modules Drastically?," *28th Eur. Photovolt. Sol. Energy Conf. Exhib.*, vol. 66, pp. 3099–3102, 2013, doi: 10.4229/28thEUPVSEC2013-4AV.4.26.

[3] T. Lorenz, E. Klimm, and K. A. Weiss, "Soiling and anti-soiling coatings on surfaces of solar thermal systems - Featuring an economic feasibility analysis," *Energy Procedia*, vol. 48, pp. 749–756, 2014, doi: 10.1016/j.egypro.2014.02.087.

[4] M. T. Chaichan, B. A. Mohammed, and H. A. Kazem, "Performance Based on Experimental Study," *Int. J. Sci. Eng. Res.*, vol. 6, no. 4, pp. 594–601, 2015.

[5] H. G. Hameed *et al.*, "Study the effect of dust on performance of PV panel and design cleaning system," *Int. J. Energy Environ. Found.*, vol. 10, no. 3, pp. 119–126, 2019.

[6] H. J. Gwon *et al.*, "Superhydrophobic and antireflective nanograss-coated glass for high performance solar cells," *Nano Res.*, vol. 7, no. 5, pp. 670–678, 2014, doi: 10.1007/s12274-014-0427-x.

[7] S. Y. Heo *et al.*, "Bifunctional moth-eye nanopatterned dye-sensitized solar cells: Light-harvesting and self-cleaning effects," *Adv. Energy Mater.*, vol. 4, no. 3, pp. 1–7, 2014, doi: 10.1002/aenm.201300632.

[8] K. Y. Law, "Definitions for hydrophilicity, hydrophobicity, and superhydrophobicity: Getting the basics right," *J. Phys. Chem. Lett.*, vol. 5, no. 4, pp. 686–688, 2014, doi: 10.1021/jz402762h.

[9] M. Ma and R. M. Hill, "Superhydrophobic surfaces," *Curr. Opin. Colloid Interface Sci.*, vol. 11, no. 4, pp. 193–202, 2006, doi: 10.1016/j.cocis.2006.06.002.

[10] A. Fernández *et al.*, "Hierarchical surfaces for enhanced self-cleaning applications," *J. Micromechanics Microengineering*, vol. 27, no. 4, 2017, doi: 10.1088/1361-6439/aa62bb.

[11] A. Lafuma and D. Quéré, "Superhydrophobic states," *Nat. Mater.*, vol. 2, no. 7, pp. 457–460, 2003, doi: 10.1038/nmat924.

[12] S. M. Kang, N. Ahn, J. W. Lee, M. Choi, and N. G. Park, "Water-repellent perovskite solar cell," *J. Mater. Chem. A*, vol. 2, no. 47, pp. 20017–20021, 2014, doi: 10.1039/c4ta05413j.

[13] K. S. Han, J. H. Shin, and H. Lee, "Enhanced transmittance of glass plates for solar cells using nano-imprint lithography," *Sol. Energy Mater. Sol. Cells*, vol. 94, no. 3, pp. 583–587, 2010, doi: 10.1016/j.solmat.2009.12.001.

[14] F. Vüllers *et al.*, "Self-Cleaning Microcavity Array for Photovoltaic Modules," *ACS Appl. Mater. Interfaces*, vol. 10, no. 3, pp. 2929–2936, 2018, doi: 10.1021/acsami.7b15579.

[15] F. Vüllers *et al.*, "Bioinspired Superhydrophobic Highly Transmissive Films for Optical Applications," *Small*, vol. 12, no. 44, pp. 6144–6152, 2016, doi: 10.1002/smll.201601443.

[16] A. Roslizar *et al.*, "Self-cleaning performance of superhydrophobic hot-embossed fluoropolymer films for photovoltaic modules," *Sol. Energy Mater. Sol. Cells*, vol. 189, no. May 2018, pp. 188–196, 2019, doi: 10.1016/j.solmat.2018.09.017.

[17] Y. Wang *et al.*, "Biomimetic corrugated silicon nanocone arrays for self-cleaning antireflection coatings," *Nano Res.*, vol. 3, no. 7, pp. 520–527, 2010, doi: 10.1007/s12274-010-0012-x.

[18] S. J. Choi and S. Y. Huh, "Direct structuring of a biomimetic antireflective, self-cleaning surface for light harvesting in organic solar cells," *Macromol. Rapid Commun.*, vol. 31, no. 6, pp. 539–544, 2010, doi: 10.1002/marc.200900658.

[19] Z. Huang, C. Cai, L. Kuai, T. Li, M. Huttula, and W. Cao, "Leaf-structure patterning for antireflective and self-cleaning surfaces on Si-based solar cells," *Sol. Energy*, vol. 159, no. November 2017, pp. 733–741, 2018, doi: 10.1016/j.solener.2017.11.020.

[20] B. Fritz *et al.*, "Towards mass fabrication of hot embossed plant surface texture replicas as photovoltaic cover layers," no. September 2018, p. 17, 2018, doi: 10.1117/12.2320555.

[21] R. Hünig *et al.*, "Flower Power: Exploiting Plants' Epidermal Structures for Enhanced Light Harvesting in Thin-Film Solar Cells," *Adv. Opt. Mater.*, vol. 4, no. 10, pp. 1487–1493, 2016, doi: 10.1002/adom.201600046.

[22] R. Schmager *et al.*, "Texture of the Viola Flower for Light Harvesting in Photovoltaics," *ACS Photonics*, vol. 4, no. 11, pp. 2687–2692, 2017, doi: 10.1021/acsphotonics.7b01153.

[23] B. Fritz *et al.*, "Upscaling the fabrication routine of bioreplicated rose petal light harvesting layers for photovoltaic modules," *Sol. Energy*, vol. 201, no. September 2019, pp. 666–673, 2020, doi: 10.1016/j.solener.2020.03.020.

[24] Z. Huang, S. Yang, H. Zhang, M. Zhang, and W. Cao, "Replication of Leaf Surface Structures for Light Harvesting," *Sci. Rep.*, vol. 5, pp. 1–10, 2015, doi: 10.1038/srep14281.

[25] S. Lee, D. Kim, and W. Hwang, "Artificial lotus leaf structures made by blasting with sodium bicarbonate," *Curr. Appl. Phys.*, vol. 11, no. 3, pp. 800–804, 2011, doi: 10.1016/j.cap.2010.11.075.

[26] S. E. Lee, K. W. Lee, J. H. Kim, K. C. Lee, S. S. Lee, and S. U. Hong, "Mass-producible superhydrophobic surfaces," *Chem. Commun.*, vol. 47, no. 43, pp. 12005–12007, 2011, doi: 10.1039/c1cc14489h.

[27] K. J. Cha *et al.*, "Effect of replicated polymeric substrate with lotus surface structure on adipose-derived stem cell behaviors," *Macromol. Biosci.*, vol. 11, no. 10, pp. 1357–1363, 2011, doi: 10.1002/mabi.201100134.

[28] H.-C. Jung *et al.*, "Formation of lotus surface structure for high

efficiency silicon solar cell," *Journal of the Korean Crystal Growth and Crystal Technology*, vol. 20, no. 1. pp. 7–11, 2010, doi: 10.6111/jkcgct.2010.20.1.007.

[29] Y. Yoon, D. W. Lee, and J. B. Lee, "Fabrication of optically transparent PDMS artificial lotus leaf film using underexposed and underbaked photoresist mold," *J. Microelectromechanical Syst.*, vol. 22, no. 5, pp. 1073–1080, 2013, doi: 10.1109/JMEMS.2013.2264729.

[30] X. S. Zhang, F. Y. Zhu, G. Y. Sun, and H. X. Zhang, "Fabrication and characterization of squama-shape micro/nano multi-scale silicon material," *Sci. China Technol. Sci.*, vol. 55, no. 12, pp. 3395–3400, 2012, doi: 10.1007/s11431-012-4853-2.

[31] N. A. Patankar, "Mimicking the lotus effect: Influence of double roughness structures and slender pillars," *Langmuir*, vol. 20, no. 19, pp. 8209–8213, 2004, doi: 10.1021/la048629t.

[32] "Nelumbo nucifera," 1999. https://www.rhs.org.uk/Plants/11438/Nelumbo-nucifera/Details.

[33] C. Ulbrich, G. Andreas, K. Hermans, A. Lambert, and U. Rau, "Analysis of short circuit current gains by an anti-reflective textured cover on silicon thin film solar cells," *Prog. Photovoltaics Res. Appl.*, vol. 21, pp. 1672–1981, 2013, doi: 10.1002/pip.

[34] C. Heine, R. H. Morf, and M. T. Gale, "Coated submicron gratings for broadband antireflection in solar energy applications," *J. Mod. Opt.*, vol. 43, no. 7, pp. 1371–1377, 1996, doi: 10.1080/09500349608232810.

[35] M. Jošt *et al.*, "Efficient Light Management by Textured Nanoimprinted Layers for Perovskite Solar Cells," *ACS Photonics*, vol. 4, no. 5, pp. 1232–1239, 2017, doi: 10.1021/acsphotonics.7b00138.

[36] M. Jošt *et al.*, "Textured interfaces in monolithic perovskite/silicon tandem solar cells: Advanced light management for improved efficiency and energy yield," *Energy Environ. Sci.*, vol. 11, no. 12, pp. 3511–3523, 2018, doi: 10.1039/c8ee02469c.

[37] A. Roslizar *et al.*, "Hot-embossed microcone-textured fluoropolymer as self-cleaning and anti-reflective photovoltaic module covers," *Sol. Energy Mater. Sol. Cells*, vol. 214, no. January, 2020, doi: 10.1016/j.solmat.2020.110582.

[38] A. I. M. Greer, I. Vasiev, B. Della-Rosa, and N. Gadegaard, "Fluorinated ethylene-propylene: A complementary alternative to PDMS for nanoimprint stamps," *Nanotechnology*, vol. 27, no. 15, 2016, doi: 10.1088/0957-4484/27/15/155301.

[39] J. Gardiner, "Fluoropolymers: Origin, Production, and Industrial and Commercial Applications," *Australian Journal of Chemistry*, vol. 68, no. 1. CSIRO, pp. 13–22, 2015, doi: 10.1071/CH14165.

[40] S. Zehentmaier, "Fluorthermoplaste in Filmanwendungen," *Gummi, Fasern, Kunststoffe*, vol. 68, no. 7, pp. 476–483, 2015.

[41] I. Nayshevsky, "Hydrophobic Fluoropolymer Nano-Coatings: Study of Anti-Reflective and Anti-Soiling Properties and Applications," City University of New York, 2020.

[42] I. Nayshevsky, Q. F. Xu, G. Barahman, and A. M. Lyons, "Fluoropolymer coatings for solar cover glass: Anti-soiling mechanisms in the presence of dew," *Sol. Energy Mater. Sol. Cells*, vol. 206, no. August, p. 110281, 2020, doi: 10.1016/j.solmat.2019.110281.

[43] S. Ok, J. Sheets, S. Welch, S. Kaya, A. Jalilov, and D. R. Cole, "Tuning hydrophobicity of a fluorinated terpolymer in differently assembled thin films," *J. Polym. Sci. Part B Polym. Phys.*, vol. 55, no. 8, pp. 643–657, 2017, doi: 10.1002/polb.24308.

[44] S. Ok, S. A. Furquan, Z. Khan, and A. Umran Dogan, "Near superhydrophobic-fluorinated THV fiber-like structures and fibers prepared by electrospinning," *High Perform. Polym.*, vol. 28, no. 2, pp. 206–214, 2016, doi: 10.1177/0954008315577440.

[45] Y. H. Yeong and M. C. Gupta, "Hot embossed micro-textured thin superhydrophobic Teflon FEP sheets for low ice adhesion," *Surf. Coatings Technol.*, vol. 313, pp. 17–23, 2017, doi: 10.1016/j.surfcoat.2017.01.026.

[46] M. Dadalas, "Fluorpolymere schützen Dachgewebe," *GAK - Gummi Fasern Kunststoffe*, vol. 64, no. 10, pp. 602–604, 2011.

[47] T. Senn, "Process development for nanostructuring and 3D micro-nanointegration," Technische Universität Berlin, 2012.

[48] M. Worgull, *Hot embossing: theory and technology of microreplication*, vol. 54. 2009.

[49] M. Worgull, M. Heckele, and W. K. Schomburg, "Large-scale hot embossing," *Microsyst. Technol.*, vol. 12, no. 1-2 SPEC. ISS., pp. 110–115, 2005, doi: 10.1007/s00542-005-0012-z.

[50] H. Dittrich, "Werkzeugentwicklung für das Heißprägen beidseitig mikrostrukturierter Formteile," Universität Karlsruhe (TH), 2004.

[51] H. C. Scheer and H. Schulz, "A contribution to the flow behaviour of thin polymer films during hot embossing lithography," *Microelectron. Eng.*, vol. 56, no. 3–4, pp. 311–332, 2001, doi: 10.1016/S0167-9317(01)00569-X.

[52] M. Heckele, W. Bacher, and K. D. Müller, "Hot embossing - The molding technique for plastic microstructures," *Microsyst. Technol.*, vol. 4, no. 3, pp. 122–124, 1998, doi: 10.1007/s005420050112.

[53] J. A. MacGeough, M. C. Leu, K. P. Rajurkar, A. K. M. De Silva, and Q. Liu, "Electroforming process and application to micro/macro manufacturing," *CIRP Ann. - Manuf. Technol.*, vol. 50, no. 2, pp. 499–514, 2001, doi: 10.1016/S0007-8506(07)62990-4.

[54] A. Kolew, D. Münch, K. Sikora, and M. Worgull, "Hot embossing of micro and sub-micro structured inserts for polymer replication," *Microsyst. Technol.*, vol. 17, no. 4, pp. 609–618, 2011, doi: 10.1007/s00542-010-1182-x.

[55] C. Khan Malek, J. R. Coudevylle, J. C. Jeannot, and R. Duffait, "Revisiting micro hot-embossing with moulds in non-conventional materials," *Microsyst. Technol.*, vol. 13, no. 5–6, pp. 475–481, 2007, doi: 10.1007/s00542-006-0184-1.

[56] C. Khan Malek and R. Duffait, "Packaging using hot-embossing with a polymeric intermediate mould," *Int. J. Adv. Manuf. Technol.*, vol. 33, no. 1–2, pp. 187–190, 2007, doi: 10.1007/s00170-006-0595-2.

[57] D. Yoo, S. Garud, D. A. C. Becker, and H. Berlin, "Lotus Leaf Structured Foils for Light Management and Self-cleaning in Liquid Phase Crystallized Silicon Thin-film Solar Cells," *IEEE PVSC Conf. Proc.*, 2021.

[58] N. Preissler *et al.*, "Impact of dielectric layers on liquid-phase crystallized silicon solar cells," *IEEE J. Photovoltaics*, vol. 8, no. 1, pp. 30–37, 2018, doi: 10.1109/JPHOTOV.2017.2768960.

[59] C. T. Trinh, R. Schlatmann, B. Rech, and D. Amkreutz, "Progress in and potential of liquid phase crystallized silicon solar cells," *Sol. Energy*, pp. 75–83, 2018, doi: 10.1016/j.solener.2017.12.041.

[60] S. Garud *et al.*, "Towards High Solar Cell Efficiency with Low Material Usage: 15% Efficiency with 14 µm Polycrystalline Silicon on Glass," *Sol. RRL*, vol. 2000058, pp. 1–8, 2020, doi: 10.1002/solr.202000058.

[61] S. Garud *et al.*, "Laser firing in silicon heterojunction interdigitated back contact architecture for low contact resistance," *Sol. Energy Mater. Sol. Cells*, vol. 203, no. i, 2019, doi: 10.1016/j.solmat.2019.110201.

[62] S. Garud, M. Bokalic, C. T. Trinh, B. Rech, D. Amkreutz, and M. Topic, "Analysis of Surface Passivation and Laser Firing on Thin-Film Silicon Solar Cells Via Light-Beam Induced Current," *IEEE J. Photovoltaics*, vol. 10, no. 5, pp. 1246–1253, 2020, doi: 10.1109/JPHOTOV.2020.3001908.

[63] R. Santbergen, T. Meguro, T. Suezaki, G. Koizumi, K. Yamamoto, and M. Zeman, "GenPro4 Optical Model for Solar Cell Simulation and Its Application to Multijunction Solar Cells," *IEEE J. Photovoltaics*, vol. 7, no. 3, pp. 919–926, 2017, doi: 10.1109/JPHOTOV.2017.2669640.

[64] M. K. Yang, "Optical properties of Teflon® AF amorphous fluoropolymers," *J. Micro/Nanolithography, MEMS, MOEMS*, vol. 7, no. 3, p. 033010, 2008, doi: 10.1117/1.2965541.

[65] M. Worgull, A. Kolew, M. Heilig, M. Schneider, H. Dinglreiter, and B. Rapp, "Hot embossing of high performance polymers," *Microsyst. Technol.*, vol. 17, no. 4, pp. 585–592, 2011, doi: 10.1007/s00542-010-1155-0.

[66] D. Murakami, H. Jinnai, and A. Takahara, "Wetting transition from the cassie-baxter state to the wenzel state on textured polymer surfaces," *Langmuir*, vol. 30, no. 8, pp. 2061–2067, 2014, doi: 10.1021/la4049067.

[67] W. Barthlott and C. Neinhuis, "Purity of the sacred lotus, or escape from contamination in biological surfaces," *Planta*, vol. 202, no. 1, pp. 1–8, 1997, doi: 10.1007/s004250050096.

[68] C. W. Extrand and S. I. Moon, "Repellency of the lotus leaf: Contact angles, drop retention, and sliding angles," *Langmuir*, vol. 30, no. 29, pp. 8791–8797, 2014, doi: 10.1021/la5019482.

[69] R. Vismara, N. O. Länk, R. Verre, M. Käll, O. Isabella, and M. Zeman, "Solar harvesting based on perfect absorbing all-dielectric nanoresonators on a mirror," *Opt. Express*, vol. 27, no. 16, p. A967, 2019, doi: 10.1364/oe.27.00a967.

[70] R. Vismara, O. Isabella, and M. Zeman, "Back-contacted BaSi_2

solar cells: an optical study," *Opt. Express*, vol. 25, no. 8, p. A402, 2017, doi: 10.1364/oe.25.00a402.

[71] M. Zeman, R. A. C. M. M. Van Swaaij, J. W. Metselaar, and R. E. I. Schropp, "Optical modeling of a-Si:H solar cells with rough interfaces: Effect of back contact and interface roughness," *J. Appl. Phys.*, vol. 88, no. 11, pp. 6436–6443, 2000, doi: 10.1063/1.1324690.